# Cooperative liquid-crystal alignment generated by overlaid topography

Youngwoo Yi, Joseph E. Maclennan, and Noel A. Clark

Phys. Rev. E **83**, 051708 — Published 24 May 2011

DOI: 10.1103/PhysRevE.83.051708

# Cooperative Liquid Crystal Alignment Generated by Overlaid Topography

Youngwoo Yi, Joseph E. Maclennan, and Noel A. Clark*

Department of Physics and Liquid Crystal Materials Research Center

University of Colorado

Boulder, Colorado 80309, USA

Abstract

Nematic and smectic liquid crystals were introduced into micron-scale gaps between plates coated with polymer films nanoimprinted with parallel arrays of rectangular channels. Overlaying of the channels on the two plates close enough at a slight angle produces a mosaic of planar / homeotropic and hybrid alignments, showing that complex liquid crystal orientation patterns can be achieved by combining two simple topographic patterns. These alignment patterns are attributed to spatial variation of surface roughness and 3D topographic structure created by a sufficient proximity of the two patterns.

**PACS Numbers**: 61.30.Hn, 61.30.Pq, 81.16.Nd, 81.65.Cf

* Correspondence email: noel.clark@colorado.edu

*Introduction*

Understanding and controlling the molecular orientation of liquid crystals (LCs) at interfaces is scientifically challenging and technologically important. Current LC devices such as displays require specific and predictable LC alignment characteristics [1-5] and future LC applications, such as in organic photovoltaics (OPV), will depend on effective alignment of novel materials systems [6]. In the latter case, for example the discotic and polymeric composite systems under development can be difficult to orient in electrically efficient geometries, a problem complicated by the nanoheterogeneity required for efficient PV performance.

One classic LC alignment mechanism enjoying a resurgence in interest is the exploitation of the coupling of the LC orientation field to surface topography, the latter inducing orientational deformation that can be minimized in energy for a particular mean orientation [7]. Recent advances in lithographic techniques for the topographic patterning of surfaces, such as AFM lithography [8] and nanoimprint lithography [9], enable the ready fabrication of patterns that can be used for LC alignment in a variety of ways. Spatial variation of the topography can produce patterns of orientation domains not achievable using standard techniques such as rubbing or oblique evaporation. Experiments with LCs in cells made of a topographically patterned plate and a non-aligning plate show a variety of alignments (i) parallel channels align the director **n**, the local mean molecular long axis direction, along the channels [10]; ii) checkerboard patterns give in-plane bistable [11], tilted [12], or homeotropic alignment [12], depending on the pattern depth; (iii) patterns of alternating channel orientation produce spatially varying director field and controllable pretilt [13]; (iv) patterns of square posts induce

bistable, tilted alignment [1]; and (v) noncentro-symmetric patterns induce a surface electroclinic effect [14]. Uncovered LC-filled channels exhibit periodic organization of smectic defects [15]. There have also been demonstrations of alignment in cells in which both plates are topographically patterned, showing uniform planar alignment and stabilization of the twisted nematic geometry [16].

Here we demonstrate a new realm in the topographic organization of LC phases, showing that for cells in which both plates are topographically patterned, distinct organizational transitions can be produced in chosen locations if the LC layer is sufficiently thin. With these transitions of the cell, the organization adopted locally must be considered as a collective response to the particular local combination of three dimensional (3D) topography of the opposing surfaces, rather than the simple response of bulk LC to aligning plates. Controlling the 3D topography offers opportunities for generating complex alignment patterns and functionalities, with stable orientation domains combined with switchable multistable regions and domains of varying birefringence or other optical and elastic properties.

These possibilities are demonstrated here by exhibiting basic cooperative topography-induced reorganization transitions of nanoconfined nematic and smectic LC phases between plates with a simple geometry of crossed linear channels nanoimprinted in rectangular cross-sections. With a sufficiently small gap between the plates, channel-induced uniform alignment favored by the channels in thick cells gives way to a mosaic of planar / homeotropic and hybrid orientations stabilized by the 3D topography.

*Experiment and Results*

Glass slides coated with polymer films having topographic surface patterning consisting of arrays of parallel rectangular channels were made by UV thiol-ene photopolymerization of monomers under pressure between the slide and a mold with channels etched into a fused silica slide [17]. The area of each channel array on the polymer was $0.2 \times 1$ mm$^2$, and five such arrays were arranged in adjacent sections with a 2 μm gap to give an overall patterned area of 1 mm$^2$. AFM analysis of the polymer surface showed that the channels have a width, separation, depth, and pitch of w = 0.8 μm, s = 0.7 μm, p = w + s =1.5 μm, and d = 0.5 μm, respectively (Fig. 1a). AFM also showed that the top surface of the separators between the channels was left substantially rougher than the channel bottoms (insets, Fig. 1a), an important characteristic for obtaining the alignment transitions reported here.

Such topographic channels are effective in aligning nematic LCs, giving director orientation parallel to the channel direction in cells with the LC between a topographically patterned surface and a random planar one [17]. This orientation is maintained in smectic A (SmA) phase obtained by cooling an aligned nematic between a patterned and random planar surface. However, LC materials exhibiting a direct transition from isotropic to SmA do not align well in cells having a single patterned surface. In an effort to improve the alignment effects of the patterning, cells were prepared with patterns on both surfaces. When the channels are overlaid almost parallel, a classical Moiré pattern, shown in the transmitted light microscope image of an empty cell (Fig. 1b) is generated, corresponding to distinct overlap conditions of the patterns. The channels on one plate are alternately opposite or in-between those on the other plate, as shown in the cross-sections in Fig. 1c, producing the transverse horizontal bands with

optical contrast shown in Fig. 1b. The pitch, $\prod$, of the Moiré pattern depends on the relative azimuthal orientation, $\theta$, of the channels, varying as $\prod \sim 1/\theta$ , with $\prod \sim 45\ \mu$m as in Fig. 1b indicating $\theta = 1.9°$ The cell gap, g, between the replicas (Fig. 1c) was varied in the range $0.2\ \mu m < g < 4\ \mu m$.

The cells were filled with 11CB (4-undecyl-4′-cyanobiphenyl) in the isotropic phase using capillary action. The LC material 11CB, which has the phase sequence I–52 ºC –SmA–44 ºC–X in thin cells [18], was chosen because of its direct isotropic to SmA transition, and its similarity to the cyano-biphenyls used in previous experiments [11, 12,17]. The LC orientation was probed using depolarized transmission light microscopy (DTLM), which reveals the orientation of **n**, the local uniaxial optic axis and layer normal in the SmA phase. The optical retardance of the cells was measured using a variable compensator and color filters. The thickness (t = d + g) of the cells was calculated from the retardance taking $\Delta n = 0.15$ for the birefringence of the LC and assuming **n** to be parallel to the substrate in the planar aligned cases.

The DTLM images of filled cells cooled slowly (at 0.02 ˚C/min) from the isotropic to the SmA phase show a strong dependence of the alignment on the cell gap, g, as illustrated in Figs. 2 a-c. In thick cells ($g > \sim 2\ \mu m$), only partial alignment is achieved, with SmA batonnets growing in a variety of orientations [19]. As the cell gap is decreased, the growth of the SmA domains is increasingly controlled by the patterning and the alignment improves, such that for $g = \sim 1\ \mu m$, where the cell gap is comparable to channel width w, a highly oriented texture with **n** parallel to the channels is obtained (Fig. 2b). In very thin cells ($g = \sim 0.2\ \mu m$), in the limit that the replicas are almost in contact, a striking orientation transition has occurred, to a state exhibiting periodic bright

and dark bands having the period of the underlying Moiré pattern and **n** parallel to the channels. The same orientation transitions were observed in nematic phase of a very thin 8CB cell (inset in Fig. 2c). The good extinction for polarizer parallel to the channels indicates that the in-plane component of **n** is parallel to the channels for the cells with gaps comparable to or smaller than the channel width, as shown in Figs. 2 b-c.

The nucleation and growth of the SmA phase from isotropic in very thin 11CB cells show interesting dynamics occurring as successive waves of spatially isolated domains, shown in Figs. 3a-c. The domains nucleate in the bright bands and grow as needles along single channels and stop when they approach the centers of the adjacent dark bands, where shifts from overlapping of the channels to overlapping of separators occur (see Fig. 4d). When one set of needles are fully-grown, new nuclei are likely to appear in random places. This temporal nucleation and growth cycle was analyzed by monitoring the growth of individual nuclei using an image analysis program. As shown in Fig. 3d, clearly, nucleation is more frequent once the existing smectic needles are almost fully grown (t ~300 s). This cycle occurred repeatedly with a period of ~300 s until all of the material in the cell underwent the transition. When the cooling rate was increased by a factor of two, the period decreased by half. We suggest that the observed temporal periodicity is due to the emission of latent heat by the growing domains during the phase transition, temporarily suppressing further nucleation in regions nearby. Inter-channel growth is suppressed in the very thin cell. In a thicker cell, in contrast, the growth of the smectic phase from the initial nuclei is continuous, both along and between the channels (the inset of Fig. 3c).

*Analysis*

To understand the dark and bright bands in very thin cells, we looked at a cell under high magnification in transmitted light with no analyzer, observing low contrast between the channels and separators in the dark bands while observed good contrast in the bright bands. This suggested that the centers of the bright bands were where the channels are in phase (I) overlapping each other, resulting in large phase difference of the transmitting light between channels and the separators; while the centers of the dark bands were where the channels were out of phase (O), i.e., shifted by a half period to overlap the separators, giving no spatial variation of cell thickness and resulting in no phase difference (see Fig. 1c).

Further study of the cells between crossed polarizer and analyzer provided quantitative information about the director orientation in I (bright) and O (dark) bands of Fig. 2c, shown in detail in Fig. 4a. The upper left inset in Fig. 4a shows a scan of the transmitted light along the thin red line in Fig. 3a for polarizer parallel and at 45° to the channels. For polarizer at 45° to the channels and light normally incident on the cell, both the centers of I and O bands transmit with optical contrast $r_{exp} = I_I / I_O \approx 4.5$, indicating some in-plane component of **n** in both bands. The transmission contrast of the two overlap geometries shown in Fig. 1c may be calculated using two different models of **n** in the channels. For **n** planar (Fig. 4b), the contrast ($r_p = P_I/P_O$) for the two bands can be calculated using the equation $P = \sin^2(\pi\Delta nt/\lambda)$, where $\lambda$ is wavelength of light, and t is the thickness of the LC film. $P_I$ is average of transmission through the in-phase channel and separator strips, with the thickness alternating between $t = 2d + g$, and $t = g$, while $P_O$ is calculated for the out-of-phase channels, with a uniform thickness $t = d + g$ (see Fig.

1c). Taking g = 0.2 μm and d = 0.5 μm, the value of $r_p$ varied from $r_p = 0.93$ ($\lambda$ = 380 nm) to $r_p = 1.35$ ($\lambda$ = 780 nm). These values are far smaller than the measured value of $r_{exp}$. Since $r_p < r_{exp}$ and the planar model gives the maximum intensity for $P_I$, a model, which gives smaller $P_O$, is required.

With homeotropic organization on the top surfaces of the separators, the director could plausibly have hybrid organization in O bands and alternation of slightly pretilted ($\delta_1$) and highly tilted ($\pi/2$-$\delta_2$) alignment from y-axis in I bands (Figs. 4c-d). This arrangement seems more plausible than a model with perfect homeotropic alignment at the top surfaces of the separators and planar at the bottom surfaces of channels, in which one would expect many inversion walls by symmetry, where the tilt of **n** changes by $\pi$, such as the example indicated in Fig. 4a and sketched in the inset. Since the cell does not show many of these defects when cooled slowly, this suggests the cell has an overall preferred tilt of **n**, resulting perhaps from a gradient in the cell thickness or in the temperature during cooling.

In this hybrid model, the effective birefringence at the center of O band calculated assuming the tilt of **n** increases linearly from 0 to $\pi/2$ between the channel bottom and the top of the separator, $n_e = 1.67$, and $n_o = 1.52$ (see Fig. 4c) is $\Delta n_h = 0.072$. The calculated contrast of the hybrid model $r_h$, using this effective birefringence at the center of O band varies from $r_h$ =3.2 ($\lambda$ = 380 nm) to $r_h = 5.4$ ($\lambda$ = 780 nm), in good agreement with the experimental measurement.

*Discussion*

To support the hybrid model, we consider nematic elastic energy of the director field in the thin cell. This will be relevant since a similar transition of the alignment in a nematic cell is observed as shown in the inset of Fig. 3c. We assume a cross section of a rough surface along an arbitrary direction in x-y plane to be a sinusoidal function for simple calculation. Then a cross section along x-direction can be expressed as a sinusoidal function $z = A\sin(qx)$, where, A and $\lambda = 2\pi/q$ are an amplitude and a period, respectively (see Fig. 5a). Then the rms roughness $R_q$ of the surface is proportional to the amplitude of the cross section, $R_q^2 = A^2/2$. If **n** is tangential to the sinusoidal surface (planar model, see Fig. 5a), the surface bend elastic energy density $\rho_s$ is proportional to the square of the roughness [7].

$$\rho_s = \frac{1}{2} k_{33} R_q^2 q^3 \tag{1}$$

We obtain surface elastic energy density of the planar model $\rho_p = 0.4$ erg/cm$^2$ using the bend elastic constant $k_{33} = 2\times10^{-6}$ dyne of 8CB [22], A = 3 nm and $\lambda = 30$ nm for the top of the separator. This elastic energy is several times larger than the measured surface anchoring energy $W_0 = 0.09$ erg/cm$^2$ of the polymer [17]. Therefore, planar anchoring of the polymer surface is no longer the dominant factor and homeotropic anchoring (see Fig. 5b) on the top of the separators can be energetically favorable because the splay elastic constant $k_{11} = 1.4\times10^{-6}$ dyne is smaller than the bend one of 8CB [20]. The surface elastic energy gain $\Delta\rho_s$ of the homeotropic alignment compared to the planar one can be calculated approximately using Beremann's formula as follows [7].

$$\Delta\rho_s \approx \frac{1}{2}(k_{33} - k_{11}) R_q^2 q^3 = 0.12 \text{ erg/cm}^2 \tag{2}$$

This gain of elastic energy, which is larger than the surface anchoring energy, can stabilize the homeotropic configuration. The energy gain per unit length of the splay organization over the bend organization is obtained by multiplying the difference between the surface energy gain and the surface anchoring energy with the width of the separator.

$$\Delta\rho_l = 2(\Delta\rho_s - W_0)s = 4.2\times10^{-6}\,dyne \tag{3}$$

Where, the factor of two is multiplied to consider the top and bottom separators.

The additional energy cost for the homeotropic model at the top of the separators is the twist elastic energy near the boundary of the separators and channels as shown in Fig. 6. The twist elastic energy density can be calculated using

$$u = \frac{1}{2}k_{22}(\nabla\mathbf{n})^2 = \frac{1}{2}k_{22}\left(\frac{\partial\delta}{\partial x}\right)^2 \tag{4}$$

where, $k_{22}$ is twist elastic constant and $\delta$ is tilt angle of director. When the cell gap is larger than the width of the separator, we assume that the twist of $\pi/2$ occurs evenly over the distance of separator width (see Fig. 6a). Then, we obtain the energy density $u = 1/2k_{22}(\pi/2)^2/s^2$ and the elastic energy per unit length is proportional to the cell gap shown as follows.

$$\rho_{l\_twist} \approx 2usg = \frac{\pi^2}{4s}k_{22}g \qquad (g \geq s) \tag{5}$$

Therefore, as cell gap increases, the total energy cost for the homeotropic organization eventually becomes larger than that of the planar one, and uniform planar alignment is favorable in thick cells as shown in Fig. 6a. When the cell gap is smaller than the width of the separator, we assume that the twist of $\pi/2$ occur evenly over the distance of the cell

gap (see Fig. 6b) and the twist elastic energy density is $u = 1/8k_{22}\pi^2/g^2$ erg/cm$^3$. The twist elastic energy per unit length can be obtained to be a constant by integrating over the blue area $g^2$ in Fig. 6b and using $k_{22} = 1\times10^{-6}$ dyne [20].

$$\rho_{l\_twist} \approx 2ug^2 = \frac{\pi^2}{4}k_{22} = 2.5\times10^{-6} \qquad (g < s) \qquad (6)$$

This twist energy is smaller than the energy gain by the splay configuration. Therefore homeotropic configuration on the top surface of the separators is energetically favorable for thin cells.

However, the planar organization is favorable on the bottoms of the channels because their rms roughness is smaller by a factor of two than the tops of the separators and the energy gain $\Delta\rho_l$ of the homeotropic organization over the planar one is negative.

The transition from I band to O band along the channels in the thin cells seems a change in topology of director field as sketched in Fig. 7. At the middle of I band, the alternation of planar and homeotropic organization (see Fig. 7a) is plausible as explained previously. As the overlapping of the separators and the channels is increased, the organization is distorted from the alternation (Fig. 7b) and a transition occurs eventually (see Fig. 7c and d) so that the organization adapts to a new topology, which is a hybrid situation (see Fig. 7e).

The transition from planar to homeotropic organization of a nematic LC on substrates by the increase of surface roughness was previously reported by Macchione and the coworkers [21]. The director tilt by the gradient of order parameters of nematic LCs on rough surfaces [22] or surface melting [23] can not explain the measured contrast between the bright and dark bands.

*Conclusions*

We demonstrated alignment transition of liquid crystals from uniform alignment to a complex alignment pattern depending on the thickness of the cells prepared by overlaying polymer films with an array of sub-micron-scale square channels. This alignment pattern is induced by cooperation of the top and bottom polymer films with a periodic variation in surface roughness once they are close enough. This suggests new approaches to making complex LC alignment patterns in a simple way, which can be applicable to tunable gratings and special arrangement of nano particles in LC-nano particle composites.

*Acknowledgements*

This work was supported by NSF MRSEC under Grant No. DMR-0820579.

*References*


1. S. Kitson and A. Geisow, Appl. Phys. Lett. **80**, 3635 (2002).
2. L. A. Parry-Jones, E. G. Edwards, S. J. Elston, and C. V. Brown, Appl. Phys. Lett. **82**, 1476 (2003); J. C. Jones, J. Soc. Info. Disp. **16**, 143 (2008).
3. S. Kuniyasu, H. Fukuro, S. Maeda, et al., Jpn. J. Appl. Phys. I **27**, 827 (1988); H. K. Hong and C. R. Seo, Jpn. J. Appl. Phys. I **43**, 7639 (2004).
4. J. P. Doyle, P. Chaudhari, J. L. Lacey, et al., Nucl. Instrum. Meth. B **206**, 467 (2003); J-H Seo, H. Jang, S. Lee, et al., Jpn. J. Appl. Phys. II **46**, L1074 (2007).
5. V. G. Chigrinov VG, H. S. Kwok, H. Hasebe, et al., J. Soc. Info. Disp. **16**, 897 (2008).
6. M. O'Neill and S. M. Kelly, Adv. Mater. **15**, 1135 (2003); R. I. Gearba, et al., Adv. Mater. **19**, 815 (2007); A. C. Mayer, et al., Adv. Funct. Mater. **19**, 1173 (2009).
7. D. W. Berreman, Phys. Rev. Lett. **28**, 1683 (1972).
8. Y. Kim and C. N. Lieber, Science **257**, 375 (1992); G. Haugstad, W. L. Gladfelter, and R. R. Jones, J. Vac. Sci. Technol. A **96**, 1864 (1996); D. W. Wang, L. M. Tsau, K. L. Wang, and P. Chow, Appl. Phys. Lett. **67**, 1295 (1995).
9. S. Y. Chou, P. R. Crauss, and P. J. Renstrom, Appl. Phys. Lett. **67**, 3114 (1995); J. Haisma, M. Verheijan, K. van den Heuvel, and Han van den Berg, J. Vac. Sci. Technol. B **14**, 4124 (1996).
10. C-H Chiu, H-L Kuo, P-C Chen, C-H Wen, Y-C Liu, and H-M P. Chen, Appl. Phys. Lett. **88**, 073509 (2006).
11. Y. Yi, M. Nakata, A. Martin, and N. A. Clark, Appl. Phys. Lett. **90**, 163510 (2007); J. S. Gwag, J-H Kim, M. Yoneya, and H. Yokoyama, Appl. Phys. Lett. **92**, 153110 (2008).

12. Y. Yi, G. Lombardo, N. Ashby, R. Barberi, J. E. Maclennan, and N. A. Clark, Phys. Rev. E **79**, 041701 (2009).

13. J. Kim, M. Yoneya, and H. Yokoyama, Nature **420**, 159 (2002); B. Zhang, F. K. Lee, O. K. C. Tsui, and P. Sheng, Phys. Rev. Lett. **91**, 215501 (2003).

14. S. Ferjani, Y. Choi, J. Pendery, R. G. Petschek, and C. Rosenblatt, Phys. Rev. Lett. **104**, 257801 (2010).

15. M. C. Choi, T. Pfohl, Z. Wen, et al., PNAS **101**, 17340 (2004); D. K. Yoon, M. C. Choi, Y. H. Kim, et al., Nat. Mater. **6**, 866 (2007).

16. Y-T Kim, S. Hwang, J-H Hong, and S-D Lee, Appl. Phys. Lett. **88**, 173506 (2006); M. J. Park and O. O. Park, Microelectron. Eng. **85**, 2262 (2008).

17. Y. Yi, V. Khire, C. N. Bowman, J. E. Maclennan, and N. A. Clark, J. Appl. Phys. **103**, 093518 (2008).

18. The phase transition temperature depended on the thickness of the cells and was a few degrees higher in thick cells.

19. Thick cells with 8CB (4-octyl-4'-cyanobiphenyl) showed uniform alignment due to the presence of the nematic phase between the isotropic and smectic phases (see the inset in Fig. 2a).

20. H. Hakemi, Liq. Cryst. **5**, 327 (1989).

21. M. Macchionea; G. De Filpoa; F. Iemmaa; F. P. Nicolettoa; N. Piccia; G. Chidichimo, Mol. Cryst. Liq. Cryst. **363**, 137 (2001).

22. R. Barberi and G. Durand, Phys. Rev. A **41**, 2207 (1990); G. Barbero, I. Dozov, J. F. Palierne, and G. Durand, *Phys. Rev. Lett*. 56, 2056 (1986).

23. G. Barbero and G. Durand, J. Phys. II **6**, 205 (1996).

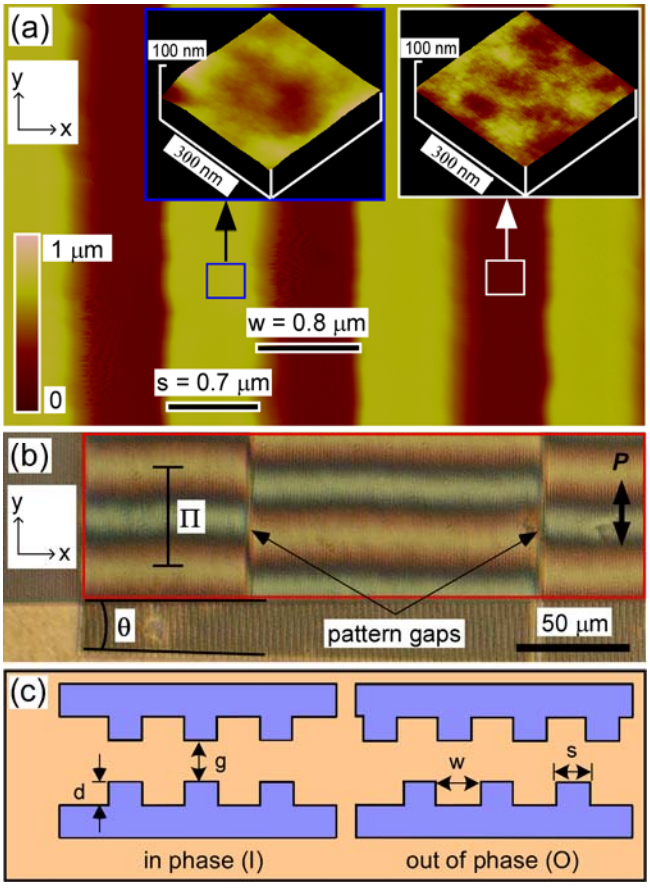


**Figure 1**. (Color online) Topographically patterned cell structures. (a) AFM images of the polymer replica. The insets show the top surface of a channel separator (left) and the bottom surface of a channel (right), with rms roughnesses of 2 nm and 1 nm, respectively. The period of the channel array is p = 1.5 μm, with each channel width w = 0.8 μm and the depth d = 0.5 μm and s = 0.7 μm is the width of the separator and g the cell gap. The channels are oriented along the y-axis. (b) Optical microscope image of an empty overlaid (inside the red box) cell in polarized light with both sets of channels aligned approximately along the y direction. The broad horizontal bands are a Moiré pattern (period Π = 45 μm), which is discontinuous at the gaps in the pattern array. (c) Cross-sections of overlaid cells, with the channels positioned in phase (I) and out of phase (O).

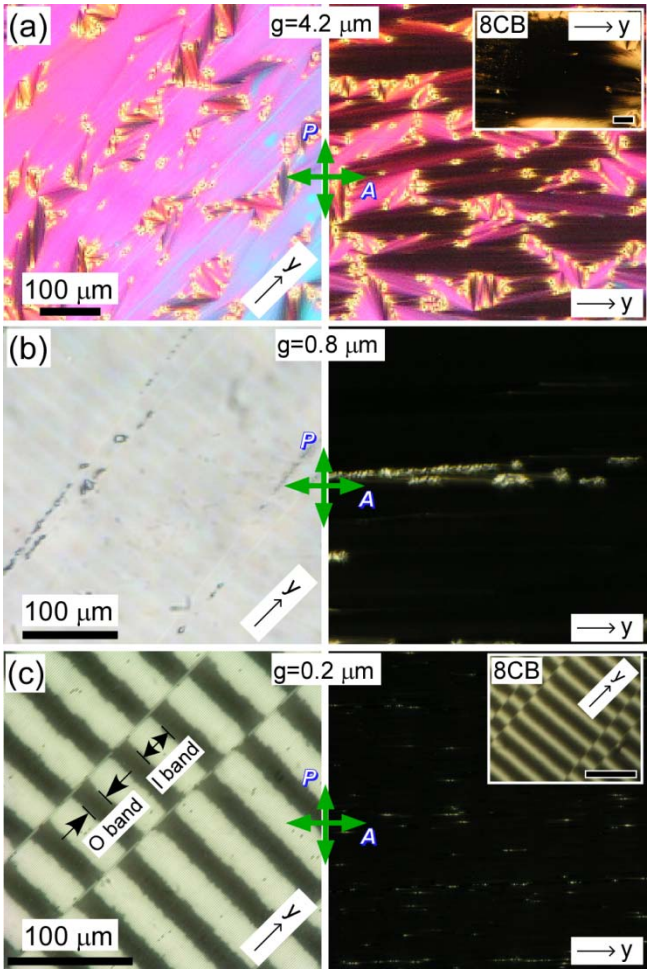


**Figure 2**. (Color online) DTLM images of 11CB cells with overlaid channels in the SmA phase. At left, the channels are rotated ~45° from the analyzer, while at right, they are approximately along the analyzer. (a) A thick cell (g = 4.2 μm) shows only partial alignment of director field. The inset shows the uniform alignment in a thicker 8CB cell with 7 μm spacers in the SmA phase. The scale bar in the inset represents 200 μm. (b) A thinner cell (g = 0.8 μm) shows uniform alignment except near the pattern gaps. (c) A very thin cell (g = 0.2 μm) shows bright and dark bands, corresponding to the Moiré pattern in Fig. 1b. The inset shows similar bands of a very thin 8CB cell in the nematic phase. The scale bar in the inset represents 100 μm.

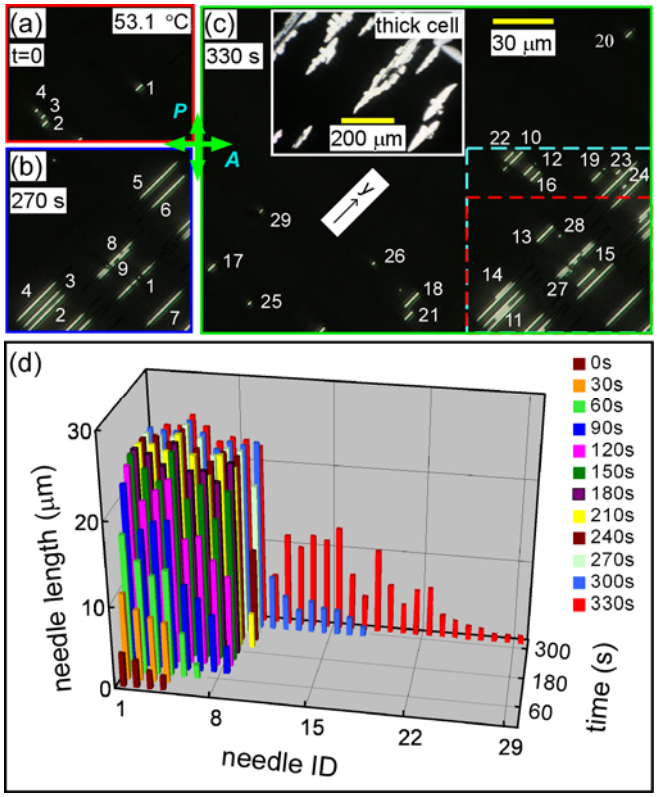


**Figure 3**. (Color online) Nucleation and growth of needle-like domains at the isotropic–SmA phase transition of 11CB in a very thin cell. DTLM pictures were obtained at intervals of 15 s while cooling a cell with g = 0.2 μm from 53.1˚C to 53.0 ˚C at 0.02 ˚C/min. Smectic domains (numbered in their order of appearance) nucleate and stop growing at the center of dark bands in the cell. (a) Four nuclei are visible at t = 0. (b) The first set of needle-like smectic domains are now fully grown (t = ~270 s). (c) Fresh set of domains are nucleated once the growth of the older needles are essentially complete (t = ~300 s). The red and cyan dashed boxes mark respectively the areas originally shown in pictures (a) and (b). The inset shows for comparison the continuous growth of SmA domains in the somewhat thicker 11CB cell (g = 0.8 μm) shown in Fig. 2b. (d) Growth dynamics of individual nuclei. Notice the appearance of many fresh nuclei at 300 s and 330 s, after the older needles are fully grown.

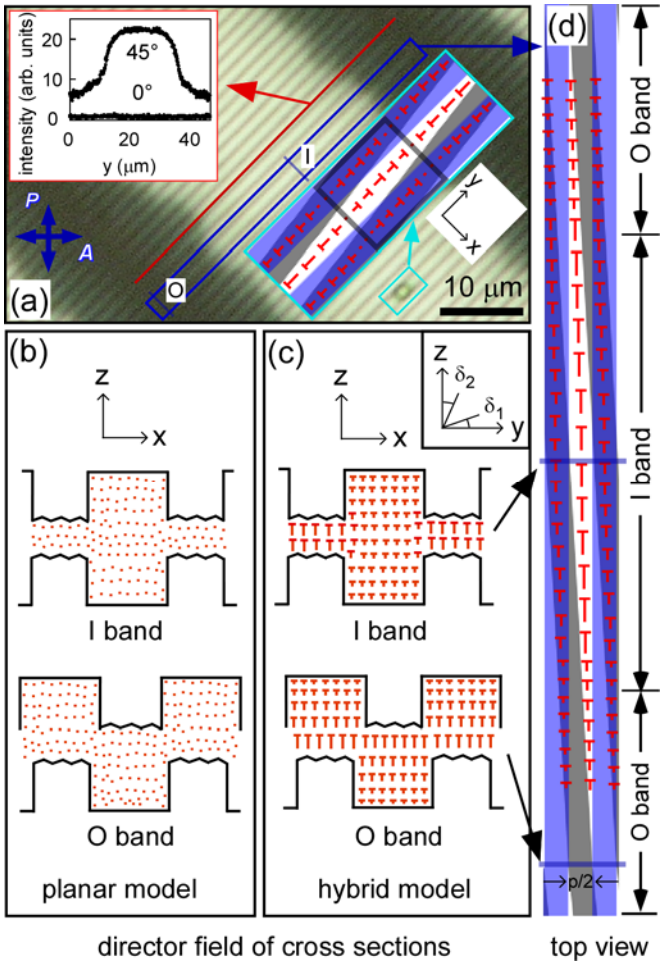


**Figure 4**. (Color online) (a) DTLM image of a thin overlaid 11CB cell showing individual channels, with a bright central I band, where the channels are mostly in phase, bounded by darker O bands. The inset shows the intensity profile along the thin red line with y-axis 45° and 0° rotated relative to the analyzer. The director field of the defect is shown in the inset indicated with a cyan box with an arrangement of thin rhombi corresponding to the four possible combinations of the top and the bottom patterns. (b) Planar director field model. In both I and O bands, **n** orients uniformly, parallel to the channels, shown here in cross-sections along the two lines, indicated with letters I and O, along x direction in the blue box in (a). The tops of the separators are rougher than the

bottoms of the channels. (c) Hybrid director field model. In I bands, **n** is uniformly pretilted by $\delta_1$ from y direction in the channels and by $\delta_2$ from z direction in the narrower gap between the separators. In O band the director tilt is non-uniform, increasing between the channel bottom and the separator surface and giving hybrid alignment. (d) Director field in the blue box shown in (a) with regions where channels (separators) overlap are sketched in the white (dark blue). At the bottom of the figure, the overlap of channels (white area) shifts by a half pitch (p/2) at the center of the O band.

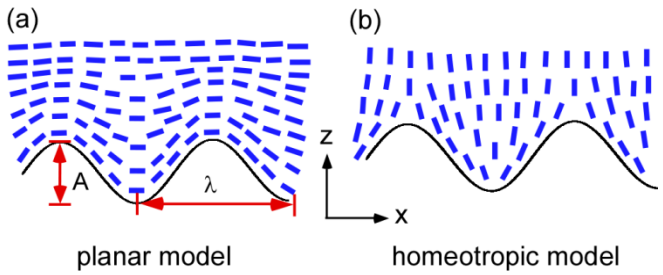


**Figure 5**. (Color online) Planar and homeotropic models on rough surface. A cross section of a rough surface along x-direction is sinusoidal, $z = A\sin(qx)$, where, A and $\lambda=2\pi/q$ are the amplitude and the spatial period, respectively. (a) Director is tangential to the sinusoidal surface and shows bend deformation. (b) Director deviates from tangent of the surface and shows splay deformation.

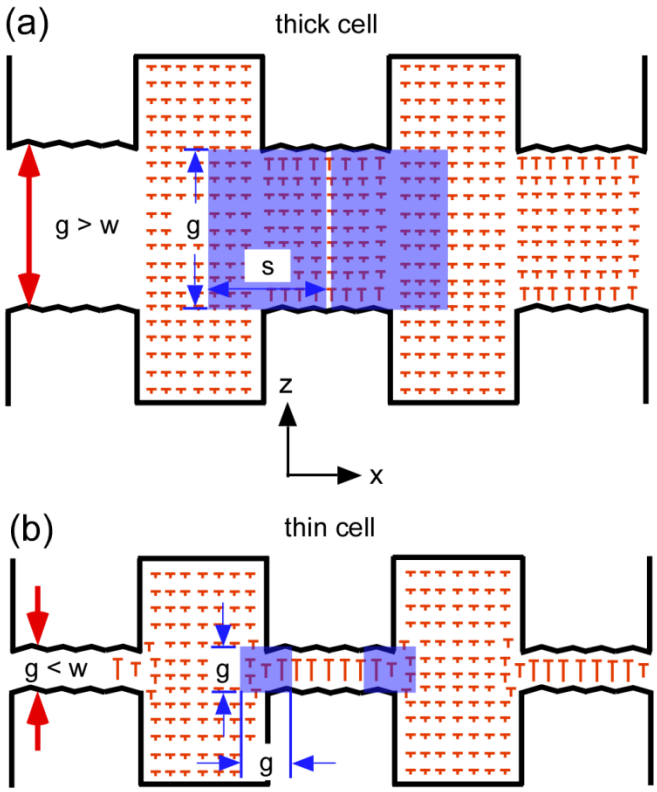


**Figure 6.** (Color online) Transition from planar alignment to alternation of planar and homeotropic alignments on the top of the separators by the decrease of the cell gap. (a) The twist elastic energy in a thick cell is too large to keep the homeotropic configuration on the top of the separators and the alignment is planar. (b) The twist elastic energy in a thin cell is small and the homeotropic anchoring on the top of separator maintains the alternation of planar and homeotropic alignment. Small pretilts are assumed in the director fields.

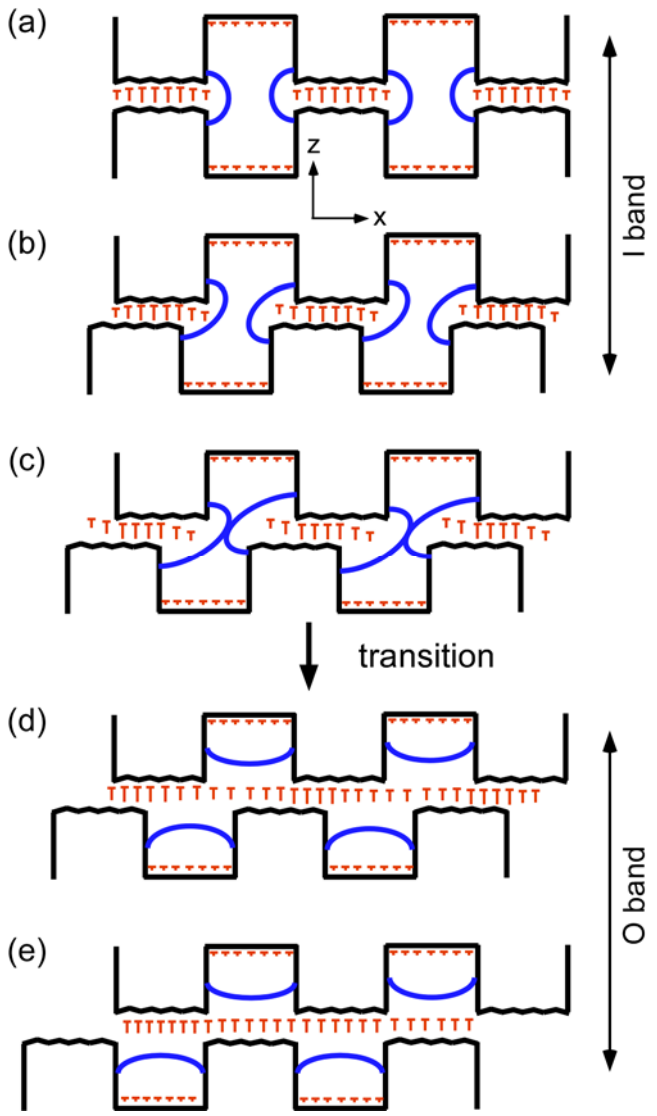


Figure 7. (Color online) Topological transition of the director field in a thin cell. As the position moves along the channels from the center of I band to that of O band a transition from the alternation of alignment (a and b) to a hybrid organization (d and e) occurs at an intermediate position (c and d). The blue curves represent contours of director field with 45° tilt from the z-axis.